ACIS UV/Optical Blocking Filter Calibration at the National Synchrotron Light Source

G. Chartas, G. Garmire, J. Nousek, L. Townsley
Department of Astronomy and Astrophysics
The Pennsylvania State University
University Park, PA 16802

ABSTRACT

Measurements of the transmission properties of the AXAF CCD Imaging Spectrometer(ACIS) UV/Optical blocking filters were performed at the National Synchrotron Light Source at Brookhaven Laboratories. The X-ray transmissions of two Al:Si/LEXAN/Al:Si three layer filters were measured between 260 and 3000 eV. The main purpose of the calibration was to determine a model transmission function with an accuracy of better than 1%. We present results from fits of model transmission functions to the measured X-ray transmission data. Detailed fine energy scans above the Al-K and C-K absorption edges revealed the presence of fine oscillations of the X-ray transmission. These features are most likely extended X-ray absorption fine structure (EXAFS). The amplitude of the EXAFS oscillations above the Al absorption edge is about 5% of the mean value of the X-ray transmission. EXAFS theory predicts a temperature dependence on the amplitude of the EXAFS oscillations.This dependence arises from the fact that thermal vibrations of the atoms in a solid produce a phase mismatch of the backscattered electron wave function. Since the ACIS filters will be at a much lower temperature on orbit we provide a prediction of the EXAFS component for the expected on orbit temperature of the ACIS filters.

Keywords: X-ray filters, filter transmission, EXAFS, X-ray telescopes, CCD, X-ray astronomy, synchrotron radiation

1 Introduction

The ACIS-I and S arrays are covered by UV/Optical blocking filters (OBF). These filters are necessary because CCD's are sensitive to UV and optical radiation (see Lumb et al., 1991). The ACIS filters consist of polyimide, a polycarbonate plastic with a chemical composition of $C_{22}H_{10}O_4N_2$, with a layer of aluminum coated on each side to provide optical light blocking. The x-ray transmission properties of the AXAF CCD Imaging Spectrometer (ACIS) UV/Optical blocking filters were measured in the energy range of 260 to 3000eV at the National Synchrotron Light Source at Brookhaven Laboratories. The main purpose of the calibration was to determine model transmission functions for the ACIS OBF's in the energy range of 0.05 to 10keV with an accuracy of better than 1%. We present a model transmission function that fits the data to better than 1% in the measured energy band of 260 to 3000 eV. The transmission above 3keV is expected to vary smoothly and is predicted by the model from the measured filter parameters. Detailed fine energy scans above the Al-K and C-K absorption edges revealed the presence of fine oscillations of the X-ray transmission. These features are most likely extended X-ray absorption fine structure (EXAFS). The amplitude of the EXAFS oscillations above the Al absorption edge is about 5% of the mean value of the X-ray transmission. The ACIS OBF's were measured at room temperature while the on orbit temperature of the filters is expected to be about -60 C. We predict that the amplitude of the EXAFS will increase by less than 0.5% when the filters are in orbit at normal operating temperatures. Optical transmission measurements on a multilayer filter composed of Al/Polyimide/Al = $330\mathring{A}/2000\mathring{A}/330\mathring{A}$ were made at PSU by Gordon Garmire, Leisa Townsley and Pat Broos. We have used the results from the optical measurements to determine the optical constants for polyimide in the measured wavelength band and predict the optical transmission performance of the flight filters.

2 Experimental Configuration

The 0.26 to 3 keV X-ray transmission of the AXAF CCD Imaging Spectrometer (ACIS) UV/optical blocking filters was measured at the National Synchrotron Light Source at Brookhaven National Laboratories. The use of the NSLS synchrotron source for the calibration was necessitated by the required high accuracy for these measurements. The NSLS provided a monochromatic X-ray beam allowing us to measure the transmission of the ACIS filters at fine energy steps with sufficient intensity for good counting statistics and fair beam stability to allow accurate detector normalization corrections.

The X-ray ring at NSLS in normal operation mode accelerates electrons to energies of about 2.5 GeV for optimized X-ray emission in the range of 1 to 10 keV. A table of the operating parameters of the NSLS X-ray storage ring is provided at their Web site (http://www.nsls.bnl.gov/). Our experiment was set up on beamline X8A, one of 56 X-ray beamlines attached to the X-ray storage ring. The beam energy incident on the filters was selected by adjusting the orientation of the crystal element of a double crystal monochromator located upstream from the vacuum chamber. Each crystal element spans a certain energy range. In particular a W/Si multilayer covers the energy range 0.26-2.0 keV with energy resolution of 2x10^{-2} a Si(111) crystal covers the range 2.1-5.9 keV with a resolution of 5x10^{-4} and a Beryl(1010) crystal covers the range from 0.8-2.0 keV with a resolution of 8x10^{-4}. In Table 1, we list the energies surveyed and the monochromator crystal elements used for the transmission measurements of the ACIS-I and ACIS-S UV/Optical blocking filters. Detailed fine energy scans were performed above the absorption K edges of C, N, O, and Al to investigate extended X-ray absorption fine structure (EXAFS) and shifts in the location of the Al-K edge due to possible Al_2O_3 contamination.

Energy Range eV	Step Size eV	Monochromator	Beam Filter	Absorption Edge
260-360	1	W/Si Multilayer	Titanium	C-K(284eV)
300-600	5	W Si Multilayer	Chromium	N-K(401.6eV)
500-660	5	W/Si Multilayer	Nickel	O-K(543.1eV)
660-860	20	W/Si Multilayer	Nickel	
800-1300	25	W/Si Multilayer	Magnesium	
1200-1600	20	W/Si Multilayer	Aluminum	Al-K(1559eV)
1450-1700	30	W/Si Multilayer	Nickel	Al-K(1559eV)
1700-2000	40	W/Si Multilayer	Nickel	Si-K(1838.9eV)
1450-1700	2	Beryl(1010)	Titanium	Al-K(1559eV)
1540-1590	0.5	Beryl(1010)	Titanium	Al-K(1559eV)
1700-2000	2	Beryl(1010)	Titanium	Si-K(1838.9eV)
2000-2600	20	Si(111)	Titanium	
2600-3000	5	Si(111)	Titanium	Cl-K(2833.0eV)

Table 1: Energies surveyed and the monochromator crystal elements used for the transmission measurements of the ACIS I and ACIS S UV/Optical blocking filters.

The configuration of the test set up is shown in Figure 1. The ACIS filters were placed into the UC/SAO spectrometer-reflectometer chamber and mounted onto a mechanical fixture. The fixture was made to support both image and spectrometer filters and was mounted on a rotary stage that allowed for the selection of the portion of the filter to be intercepted by the X-ray beam. The X-ray beam was collimated with a set of vertical and horizontal entrance slits to a size of 2mm by 2mm. The beam flux was monitored using a detector that was moved in and out of the X-ray beam with a computer controlled actuator.

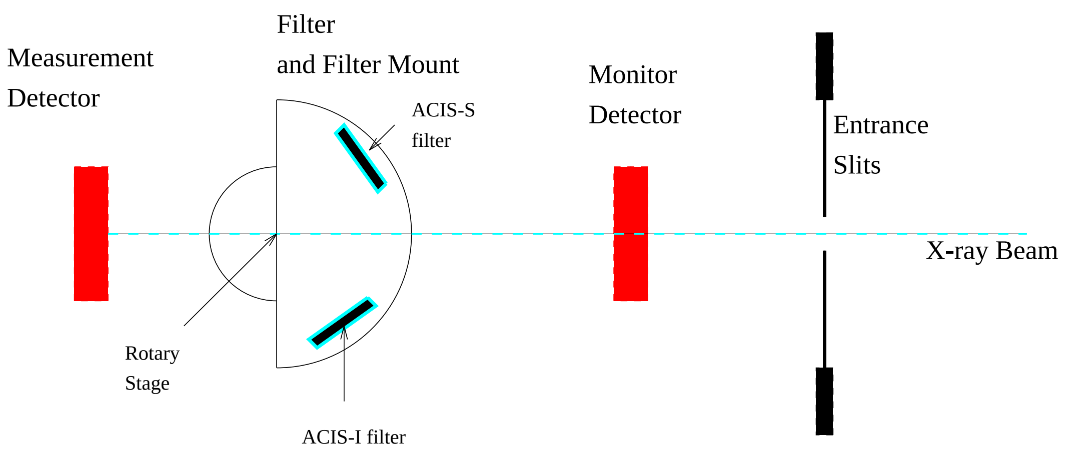

Figure 1: Schematic of the test configuration for the measurement of the X-ray transmission of the ACIS filters.

3 Calibration Strategy

The transmission of the filters is determined by moving the filter in and out of the beam and using a "measurement" detector, to measure the X-ray flux attenuated and non-attenuated by the filter respectively. The purpose of the monitor detector measurements is to take into account possible flux variations of the beam between the time the filter is in vs. when it is out of the beam. Both detectors are silicon PIN photodiodes. One detector is exposed to the X-ray beam at a time allowing a simultaneous background signal level measurement from the other unexposed detector. If $I_{i,j}$ represents a measured signal from the i'th detector (i=0 for the monitor and i=1 for the measurement detector), taken when the filter is located in the j'th position (j=in, for filter in beam, j=out, for filter out of beam), then the X-ray transmission at the X-ray energy E is determined using the expression,

$$T(E) = \frac{I_{1,in} - B_{1,in}}{I_{1,out} - B_{1,out}} \frac{I_{0,out} - B_{0,out}}{I_{0,in} - B_{\ 0,in}} \tag{1}$$

where $B_{i,j}$ is the background measurement of detector i with a filter in the j position.

Measurements with the filters out of the beam provide cross calibration of the monitor and measurement detector at all energies selected for the transmission measurements. A cross calibration between measurement and monitor detectors was performed before and after each transmission measurement. As an estimate of the errors in our measurements, we took the percent change in the two cross calibration runs. For the data points considered in the present analysis the percent change in normalization was below 0.5% . There is a delay of about 20 sec between measurements from each detector and one expects there to be an additional calibration error due to changes in the beam intensity, shape and direction that could occur during that time interval.

4 Modeling the Transmission Data and Determining an X-ray Transmission Function.

A method commonly used to model the X-ray transmission of filters assumes that the absorption through a multilayer filter with constituent compounds i is described by the equation,

$$\frac{I}{I_o} = \prod e^{-\mu_i \rho_i}, \tag{2}$$

where μ_i is the mass absorption coefficients of constituent compound i and ρ_i is the mass per unit area of the constituent compound i. μ_i can be expressed as a function of the compound's constituent elements j as,

$$\mu_i = \sum \mu_j w_j, \tag{3}$$

where μ_j is the mass absorption coefficients of element j, and w_j is the fraction by weight of element j. Tabulated values for the mass absorption coefficients for elements with atomic weights ranging from Z = 1 to Z = 92 may be found in Henke et al. (1993).

We initially performed a least squares fit to the transmission data of the Imager and Spectroscopy filters using the function given in equation (2) while considering a multilayer layer filter structure of the form Al_2O_3/Al:Si/Polyimide/Al:Si/Al_2O_3. Free parameters for this fit were the mass per unit area of Polyimide ($C_{22}H_{10}O_4N_2$) and Al. The large values for χ^2 obtained in these fits make them formally unacceptable. The residuals to these fits indicate that most of the discrepancy between the model and data occurs above the absorption edges of C, N, O, and Al. The transmission data clearly show oscillations above the absorption edges that extend up to several hundred eV. Such structures are commonly known as extended X-ray absorption fine structure and occur only when atoms are in condensed matter. The oscillations arise from interference of the scattered electron wavefunction outgoing from a central atom, i, with the backscattered electron wavefunctions from nearby atoms, j. A detailed review of EXAFS theory and applications may be found in Stern and Heald (1983).

In our next attempt to fit the transmission data we excluded energies corresponding to EXAFS and used the same function as in the previous model. The values obtained for χ^2 of ~ 0.2 (for 442 degrees of freedom) indicate a significant improvement in the fit and we obtain fitted values for the mass per unit area for the Imager filter, Polyimide of 2.734×10^{-05} gr cm^{-2} and Al of 4.071×10^{-05} gr cm^{-2} and for the Spectroscopy filter Polyimide of 2.632×10^{-05} gr cm^{-2} and Al of 3.068×10^{-05} gr cm^{-2}.

For the purpose of determining a function that fits the transmission data well, we used a very simplistic EXAFS model that incorporates features from the independent particle model developed by Stern 1978, Lee and Pendry 1975, Stern et al. 1975. Our model considers only interference effects from the nearest atomic shell.

The EXAFS component $\chi(k)$ is defined as the oscillating part of the mass absorption coefficient and is given by,

$$\chi(k) = \frac{\mu - \mu_0}{\Delta\mu_0} \tag{4}$$

where μ_0 is the smoothly varying part of the mass absorption coefficient corresponding to an isolated atom, $\Delta\mu_0$ is the change in the mass absorption coefficient over the absorption edge, and k is the wavenumber of the scattered photoelectron given by,

$$k = \frac{\sqrt{2m(E - E_{edge})}}{\hbar} \tag{5}$$

The model used to fit the oscillatory component of the transmission has the form,

$$\begin{aligned}\xi_j(E) = a_0(E - E_{j,edge})^{-\frac{1}{2}} step(E_{j,edge}, E_{j,4}) \exp\left(-a_1(E - E_{j,edge})\right) \sin\left(a_2(E - E_{j,edge})^{\frac{1}{2}} + a_3\right) step(E_{j,2}, E_{j,4}) \\ + a_4 \sin\left(a_5 E^{\frac{1}{2}} + a_6\right) step(E_{j,1}, E_{j,2}) \\ + (a_7 E + a_8) step(E_{j,3}, E_{j,4})\end{aligned} \tag{6}$$

The term $a_2(E - E_{j,edge})^{-\frac{1}{2}}$ represents the phase shift of a photoelectron as it traverses the distance 2R, where R is the interatomic separation, a_3 and $\exp(-a_1(E - E_{j,edge}))$ account for phase shifts in the presence of potentials, disorders and thermal vibrations of atoms about their average distance R from the central atom. Near edge structure in our transmission data is modeled with the term $a_4 \sin(a_5 E^{\frac{1}{2}} + a_6)$. Equation 6 does not take into account the nonlinear dependence of the phase shift and the dependence of the backscattering amplitude on k. A more physical model will be presented in a future publication.

For our modeling purposes j takes the values j=0 for the Al-K edge and j=1 for the C-K edge. We define the function $step(E_{j,1}, E_{j,2})$ as follows,

$$\begin{aligned} step(E_{j,1}, E_{j,2}) &= 0, \text{for } E_{j,1} > E \text{ or } E_{j,2} < E \\ step(E_{j,1}, E_{j,2}) &= 1, \text{for } E_{j,1} < E < E_{j,2} \end{aligned} \tag{7}$$

In Figure 2 and Figure 3 we show fits of our simple EXAFS model to the regions above the Al-K and C-K edges. Because of the limitations of the multilayer monochromator the EXAFS

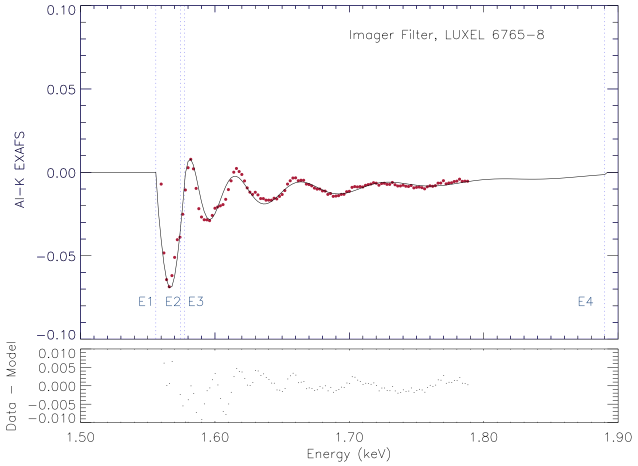

Figure 2: Top Panel; Al-K EXAFS with model fit. Lower Panel; Difference between data and model .

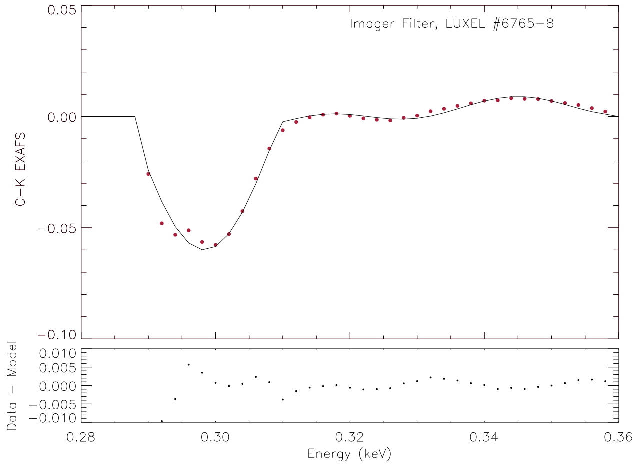

Figure 3: Top Panel; C-K EXAFS with model fit. Lower Panel; Difference between data and model .

above the N-K and O-K edge were not resolved. In Figure 2 we also show the relevant energy boundaries used in our model. $E_{j,edge}$ defines the energy of the absorption K edge, ($E_{j,2}$, $E_{j,4}$) , ($E_{j,1}$,$E_{j,2}$), ($E_{j,3}$,$E_{j,4}$), define the boundaries of the first, second and third term of equation (6) respectively.

The total transmission function of the ACIS filters is finally described by the following expression,

$$f(E) = \prod e^{-\mu_j \rho_j} + \sum \xi_j(E) step(E_{j,1}, E_{j,4}) \tag{8}$$

For energies excluding the EXAFS regions the transmission function $f(E)$ is given by the fit of our model given by equation (2) that incorporates the atomic scattering factors f_1 and f_2 as tabulated by Henke et al., (1993). For energies within the EXAFS regions our model function $f(E)$ includes in addition the best fit model to the EXAFS regions. The values for all the relevant parameters that enter equation (8) are listed in Table 2.

The transmission data for the Imager and Spectroscopy filters together with the model transmission function and the percent difference between the model and data are presented in Figure 4 and Figure 5

Filter	Fitted Parameters for Smooth Component gr cm^{-2}	Fitted Parameters for ξ_{al}(E) Component	Fitted Parameters for ξ_c(E) Component
Imager, 6765-8	$\rho_{Polyimide} = 2.73400 \times 10^{-5}$ $\rho_{al} = 4.07111 \times 10^{-5}$ $\rho_{Al_2O_3} = 7.2 \times 10^{-7}$	$a_0 = 0.00391$ $a_1 = 8.58072$ $a_2 = 71.89980$ $a_3 = 3.48600$ $a_4 = 0.05499$ $a_5 = 400.001$ $a_6 = 0.39964$ $a_7 = 0.04000$ $a_8 = -0.07724$ $E_{0,1} = 1.556$ $E_{0,2} = 1.5775$ $E_{0,3} = 1.558$ $E_{0,4} = 1.89$ $E_{0,edge} = 1.56$	$a_0 = 0.00009895$ $a_1 = -39.49626$ $a_2 = 97.56914$ $a_3 = 3.02784$ $a_4 = 0.05998$ $a_5 = 150.00030$ $a_6 = 4.46030$ $a_7 = 0.199918$ $a_8 = -0.06410$ $E_{1,1} = 0.29$ $E_{1,2} = 0.3095$ $E_{1,3} = 0.3095$ $E_{1,4} = 0.3600$ $E_{1,edge} = 0.2842$
Spectrometer,6732-8	$\rho_{Polyimide} = 2.63186 \times 10^{-5}$ $\rho_{al} = 3.06826 \times 10^{-5}$ $\rho_{Al_2O_3} = 7.2 \times 10^{-7}$	$a_0 = 0.00263$ $a_1 = 5.00026$ $a_2 = 71.79978$ $a_3 = 3.49500$ $a_4 = 0.04000$ $a_5 = 400.00003$ $a_6 = 0.40503$ $a_7 = 0.03200$ $a_8 = -0.06001$ $E_{0,1} = 1.556$ $E_{0,2} = 1.5775$ $E_{0,3} = 1.5580$ $E_{0,4} = 1.89$ $E_{0,edge} = 1.56$	$a_0 = 0.00013$ $a_1 = -39.99043$ $a_2 = 97.99200$ $a_3 = 3.00020$ $a_4 = 0.08000$ $a_5 = 145.00028$ $a_6 = 0.88018$ $a_7 = 0.34000$ $a_8 = -0.11108$ $E_{1,1} = 0.29$ $E_{1,2} = 0.3098$ $E_{1,3} = 0.3098$ $E_{1,4} = 0.36$ $E_{1,edge} = 0.2842$

Table 2: Values for parameters of ACIS Imager and Spectrometer transmission function that enter equation (8)

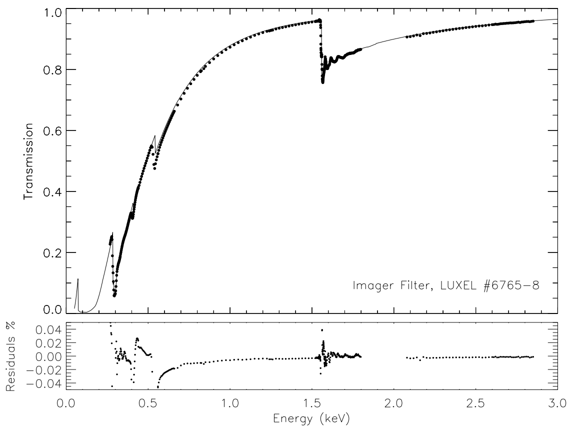

Figure 4: Top Panel; X-ray transmission data of Imager filter with best fit transmission model. Lower Panel; Percent difference between model fit and data.

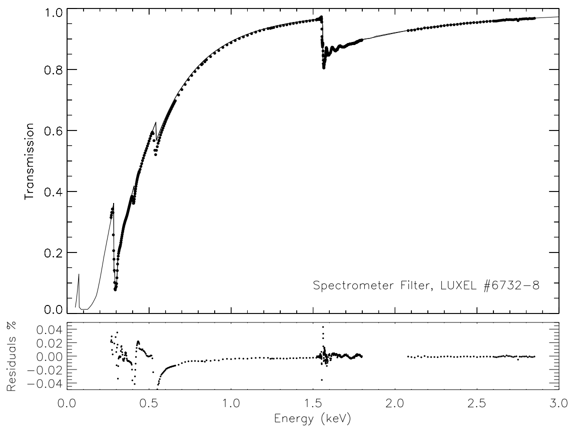

Figure 5: Top Panel; X-ray transmission data of Spectrometer filter with best fit transmission model. Lower Panel; Percent difference between model fit and data.

5 Optical Characterization of the ACIS UV/Optical Blocking Filters.

Measurements of the optical transmission of a multilayer filter composed of Al/Polyimide/Al = $330\mathring{A}/2000\mathring{A}/330\mathring{A}$ at PSU (values of multilayer thicknesses reported by LUXEL corporation) were used to constrain the optical constants for polyimide. To infer the real and imaginary parts of the refractive index from the transmission measurements we constructed a model transmission function with optical constants for polyimide parameterized as:

$$n(\lambda) = A + B/(C - \lambda)$$
$$k(\lambda) = D + E/(F - \lambda)$$

where n and k are the real and imaginary parts of the refractive index for polyimide.

The optical transmission of the ACIS multilayer filters was calculated using the matrix method described in Born and Wolf, Principles of Optics 1980.
By solving Maxwell's equations for the total electric and magnetic field with boundary conditions at the filter interfaces one finds that the relation between the incident and exiting electromagnetic fields can be written in matrix notation as :

$$\begin{pmatrix} E_I \\ H_I \end{pmatrix} = [M] \times \begin{pmatrix} E_{II} \\ H_{II} \end{pmatrix}$$

$$M = \begin{vmatrix} cos(k_0 h) & \iota sin(k_0 h)/Y_1 \\ Y_1 \iota sin(k_0 h) & cos(k_0 h) \end{vmatrix}$$

where M is the characteristic matrix of the stratified medium.

A least squares fit of a model transmission function, incorporating the above parameterization of n and k, to the measured optical transmission data provided the optical constants

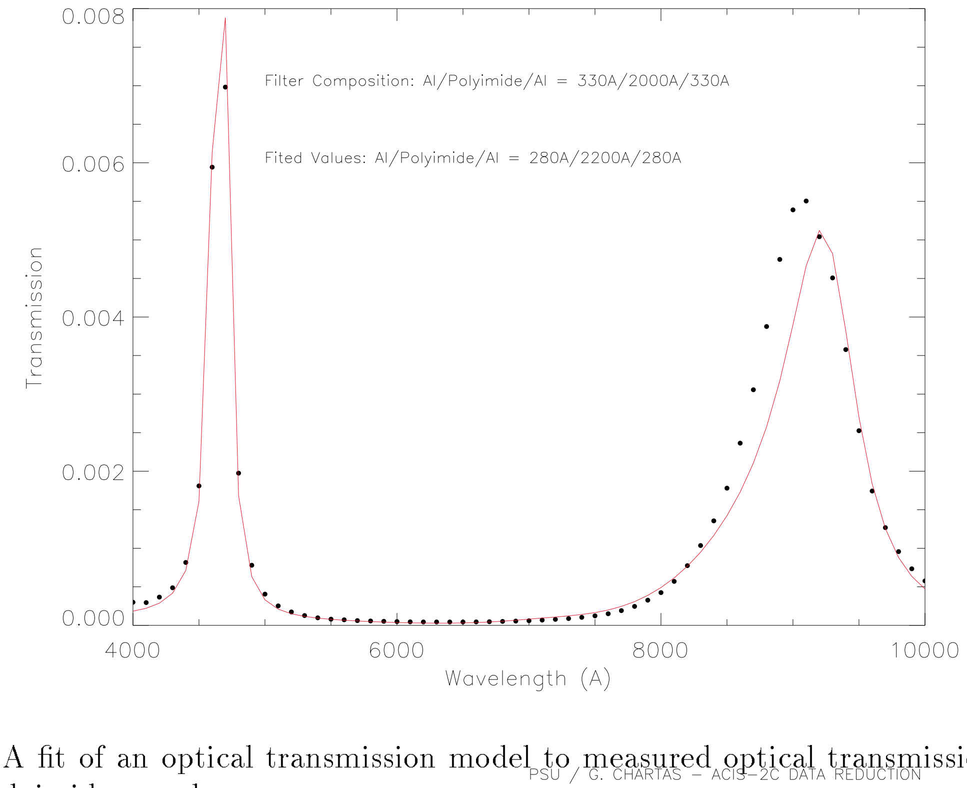

Figure 6: A fit of an optical transmission model to measured optical transmission of an aluminized polyimide sample.

for polyimide which were then used to predict the the optical transmission performance of the flight filters. In Figure 6 we present a fit of our model transmission function to the polyimide data.

Figure 7 shows the real part of the refractive index for polyimide resulting from the fit of our model to the optical transmission data for the polyimide sample.

We incorporatied the derived optical constants of polyimide into a transmission model for the ACIS-I and ACIS-S flight multilayer filters. For the simulations of the ACIS I and S transmissions we assumed the following thicknesses:

$$\text{ACIS-I : Al/Polyimide/Al} = 1200\mathring{A}/2000\mathring{A}/400\mathring{A}$$
$$\text{ACIS-S : Al/Polyimide/Al} = 1000\mathring{A}/2000\mathring{A}/300\mathring{A}$$

Figure 8 and Figure 9 show the predicted optical transmission of the ACIS-I and ACIS-S OBF's respectively. Peaks appear in the transmittance, one at about 4300 $\mathring{A}$ and the other at about 8500 $\mathring{A}$. The two peaks in the transmission curve shift toward smaller wavelengths as the incident photon angle is increased.

The amplitude of the transmission does not change significantly in the 3-7 degree range (the angle of incidence of rays at the HRMA focal point is expected to range from 3 to 7 degrees), however for large incident angles (60 degrees) the transmission at 8000A is expected to increase by about 1 order of magnitude (with respect to the normal incidence case). This effect may need to be considered especially if a large scattered optical light component is present.

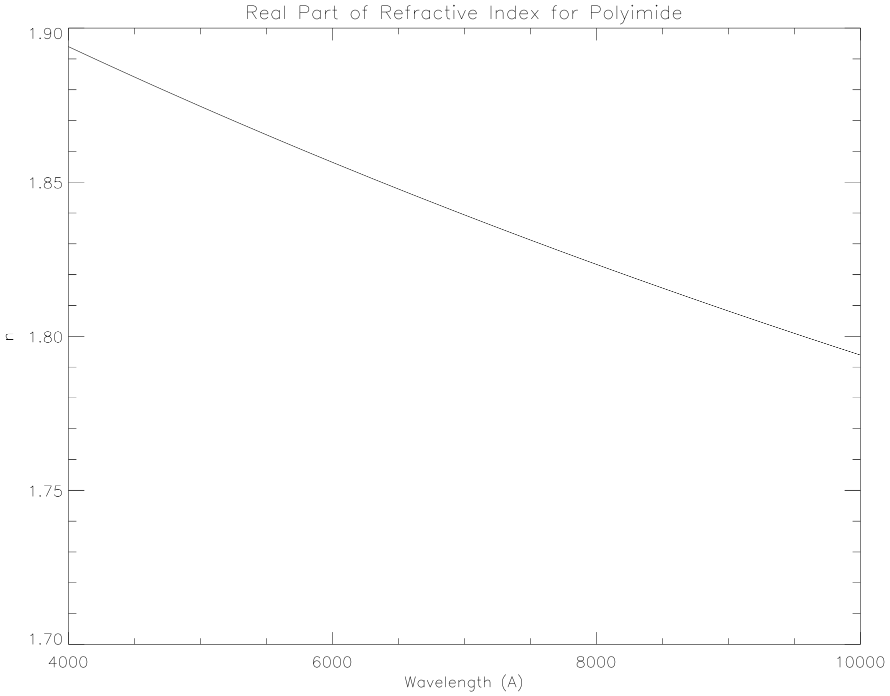

Figure 7: Real part of refractive index for polyimide.

The diffuse transmission through the ACIS UV/Optical filters was calculated using the expression:

$$T_{diff}(\lambda) = \frac{\sum(w(\theta_{n-1}, \theta_n) * T(\theta_{n-1}, \theta_n, \lambda))}{\sum(w(\theta_{n-1}, \theta_n))}$$

where :
$w(\theta_{n-1}, \theta_n) = cos(\theta_{n-1}) - cos(\theta_n)$, is a weighting function that takes into account the differential solid angle that the filter "sees" for incident photon angles between θ_n and θ_{n-1}. $T(\theta_{n-1}, \theta_n, \lambda)$ is the transmission for rays incident at an angle of θ_{n-1}. $T(\theta_{n-1}, \theta_n, \lambda)$ was calculated for incident angles of 0,1,2,...89 degrees

Figure 10 and Figure 11 show the predicted transmission including interference effects for diffuse light for the ACIS I and S OBF's respectively.

6 Temperature Dependence of Filter Properties

An issue that may be relevant to the accurate determination of the filter transmission on orbit is the temperature dependence of the amplitude of EXAFS. According to EXAFS theory the amplitude of the EXAFS oscillations are a function of temperature. This dependence arises from the fact that thermal vibrations of the atoms in a solid produce a phase mismatch of the backscattered electron wave function. The transmission properties of the ACIS filters were measured at room temperatures $\sim$ 20 C while the on orbit filter temperature is expected to be about -60 C. The temperature dependence of the EXAFS component is incorporated in a Debye-Waller type term Q(k,T) (Stern et al., 1975). For thermally induced disorders of atoms and for deviations about the average shell distance of R_j which follow a Gaussian distribution,

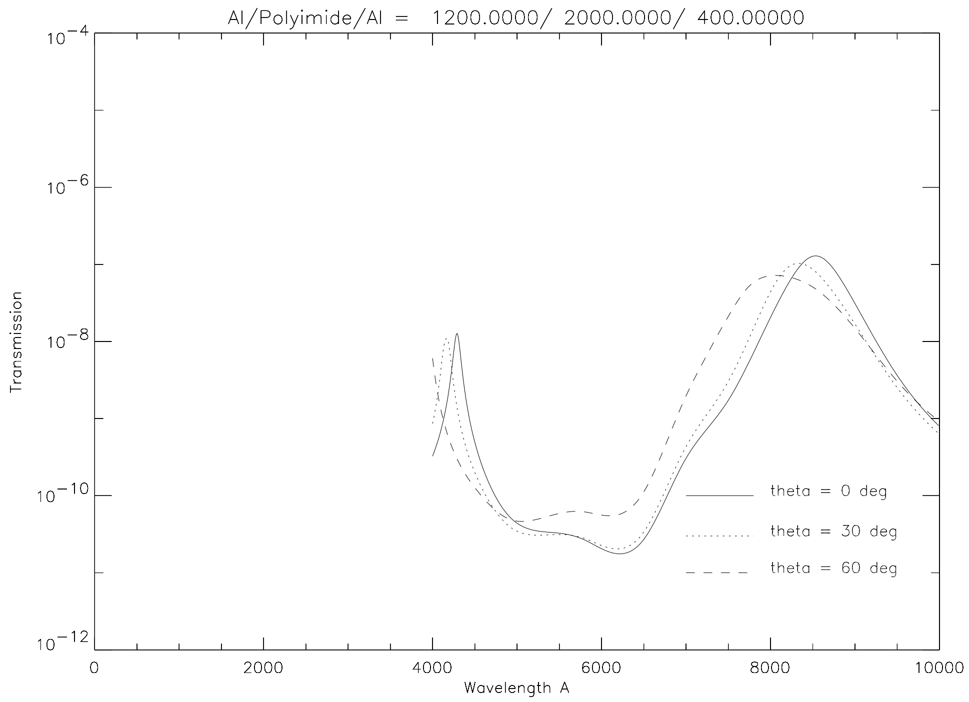

Figure 8: Predicted Optical Transmission for the ACIS I OBF for angles between photon direction and normal to CCD of 0, 30 and 60deg.

Q(k,T), is given by,

$$Q(k,T) = e^{-2k^2\sigma^2} \tag{9}$$

where σ is the mean square deviation about the average value R_j. For the Einstein model of lattice vibrations, where motions between adjacent atoms are uncorrelated σ^2 has the form,

$$\sigma^2 = \frac{\hbar}{M_r\omega}\frac{1}{e^{\frac{\hbar\omega}{kT}} - 1} \tag{10}$$

where M_r is the reduced mass and ω is the frequency of vibration of the atoms and is related to the Einstein temperature of the solid through the expression,

$$\omega = \frac{T_{ein}k}{\hbar} \tag{11}$$

To derive the temperature dependence of the filter transmission we assume that $\chi(k) = C(k)Q(k,T)$. If we define f_{sm} as the smooth component of the transmission function, (as defined in section 5), and f_{tot} as the total transmission function then using the above assumption and equation (4) we obtain,

$$\frac{f_{tot}(T)}{f_{sm}(T)} = e^{-\rho(\mu-\mu_0)} = e^{-\rho\mu_0\chi(k)} = e^{-\rho\mu_0 C(k)Q(k,T)} \tag{12}$$

and solving for C(k) we have,

$$C(k) = -\frac{1}{\rho\mu_0}\frac{\ln\left(\frac{f_{tot}(T_{gr})}{f_{sm}}\right)}{Q(k,T_{gr})} \tag{13}$$

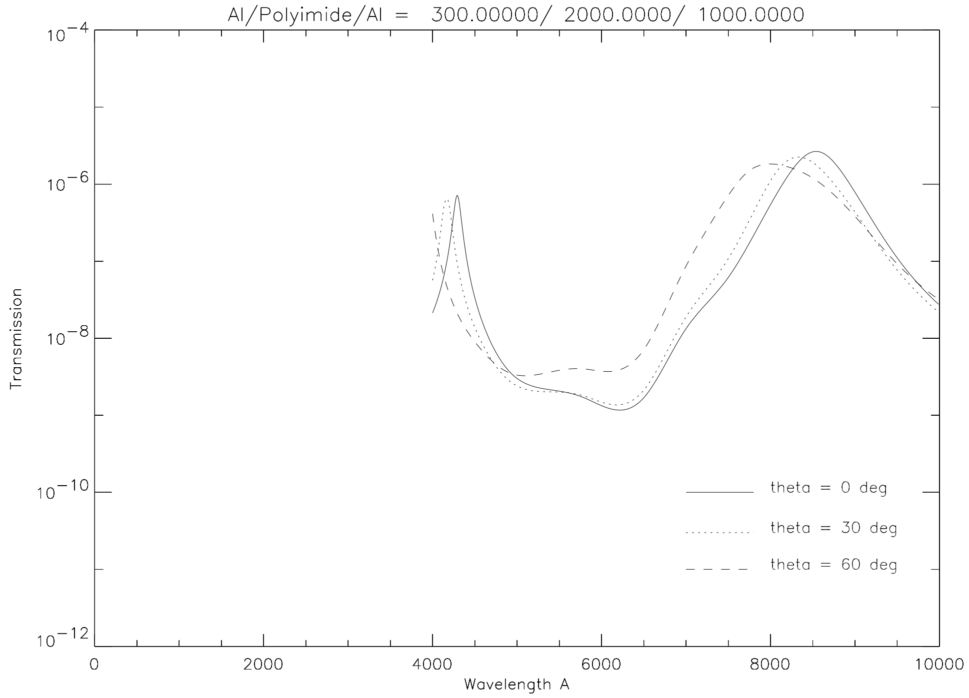

Figure 9: Predicted Optical Transmission for the ACIS S OBF for angles between photon direction and normal to CCD of 0, 30 and 60deg.

The on orbit transmission at temperature T_{orb} is expressed as a function of the transmission as measured on ground at temperature T_{gr} by the expression,

$$\frac{f_{tot}(T_{orb})}{f_{tot}(T_{gr})} = e^{-C(k)\rho\mu_0[Q(k,T_{orb})-Q(k,T_{gr})]} \tag{14}$$

In Figure 12 we show the percent change in filter transmission above the Al-K absorption edge for an expected on orbit filter temperature of -60 C.

7 Summary and Conclusions

The X-ray transmission of the ACIS-I and ACIS-S flight-like filters was measured at NSLS in the energy range between 0.26 and 3 keV. We have presented a means of constructing an X-ray transmission function for the ACIS Imager and Spectrometer filters that can be expressed as a function of atomic scattering factors and EXAFS effects. The transmission function follows the data to better than 0.5% in non-XAFS regions and better than 1% in the c-K and al-K EXAFS regions. For energies within several eV of the absorption edges, larger deviations of a few percent are observed. These can be explained as a combination of the limits in the resolving power of the monochromator used in our measurements, the uncertainties in the atomic scattering factors near absorption edges and to the presence of resonance lines and narrow near edge X-ray absorption structure within several eV of the absorption edges. A detailed investigation of the spatial uniformity of the ACIS filter performed by Townsley et al. 1996 show the ACIS filter X-ray transmission uniformity to be better than 2% over the entire filter area, down to spatial scales of $\sim$ 1mm. Finally as our future scientific goals for X-ray observations become

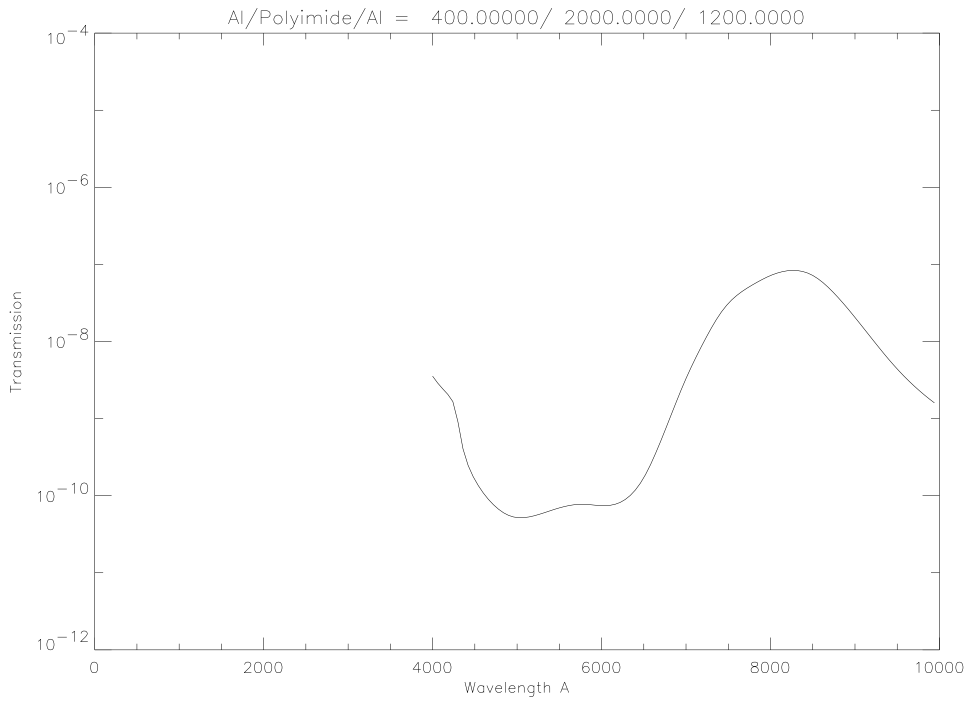

Figure 10: Predicted Optical transmission for the ACIS I OBF for diffuse illumination.

even more demanding subtle effects such as temperature dependence of EXAFS will need to be considered. We presented a simple model to describe the change in the X-ray transmission of a filter with temperature and estimated a change of less than 0.5% in the amplitude of the al-K EXAFS for the ACIS filters for temperatures ranging from 20 C to -60 C.

We would like to thank Pat Broos, Catherine Grant, Zhiyu Guo, Doug Kelly for supporting the calibration of the ACIS filters at NSLS and Lars Furenlid for providing software for the EXAFS analysis. This work has been supported at PSU by NASA contract NAS8-38252.

References

Henke, B. L., Gullikson, E. M., and Davis, J. C., 1993, Atomic Data and Nuclear Data Tables, 1993, Vol. 54 No. 2.

Lee, P. A., & Pendry, J. B., 1975, Phy. Rev. B11, 2795.

Lumb, D.H., Berthiaume, G. D., Burrows, D. N., Garmire, G. P., Nousek, J. A., Experimental Astronomy, 1991, 2, 179.

Powell et al., Opt. Eng., 1990, Vol. 29, No. 6.

Stern, E. A., Heald S. M., *Handbook on Synchrotron Radiation* V 1B, ERNST-ECKHARD KOCH, 1983.

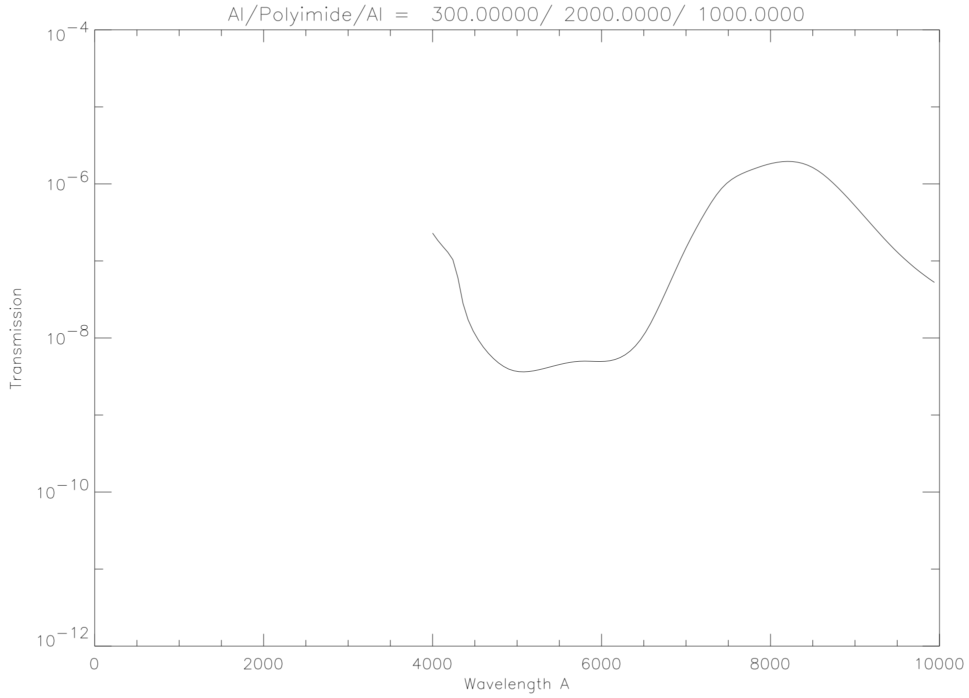

Figure 11: Predicted Optical transmission for the ACIS S OBF for diffuse illumination.

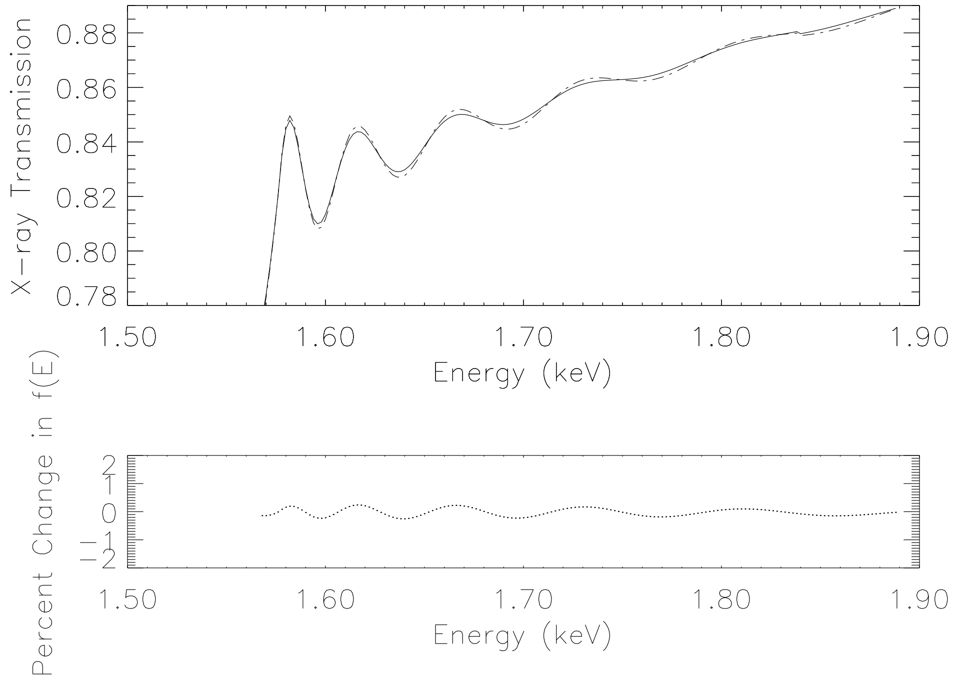

Figure 12: Top Panel; Filter transmission of Spectrometer filter above the Al-K absorption edge at 20 and -60 C. Lower Panel; Percent change in filter transmission between 20 and -60 C